# Scattering approach to semiconductor double quantum dot cavities

W. Pötz
*Institut für Physik, Karl-Franzens-Universität Graz, Universitätplatz 5 8010 Graz, Austria*
(Received 22 August 2007; published 9 January 2008)

The interaction of a coherent light field with two adjacent two-sided cavities, each containing a semiconductor quantum dot which is charged by a single excess electron, is studied within *S*-matrix theory. Dissipation in the nonresonantly driven dots and intercavity losses are treated phenomenologically. Light transmission is studied as a function of the initial state of the quantum dots (QDs), light polarization, dissipative losses, as well as dissimilarities between the two QD cavities. The transmission spectrum consists of a superposition of resonances from the individual cavities and Fabry-Pérot-like resonances associated with the double cavity. Faraday rotation and phase shifts caused by the nonresonantly driven trion transition allow nondestructive distinction between parallel "up," "down," and antiparallel spin orientation for the two excess electrons for identical cavities. With increasing asymmetry between the two cavities, the transmission spectrum reveals more and more the initial spin orientation of the individual electrons. Selection of the center frequency and duration of the incident laser pulse allows us to reveal preferentially either the relative spin orientation, needed as prerequisite for entanglement generation, or the orientation of individual spins. A quantitative estimate of the effects on the transmitted light arising from various physical sources of dissimilarities, as well as the effect from remote transitions, is given for typical system parameters.

DOI: 10.1103/PhysRevB.77.035310 PACS number(s): 73.21.La, 78.67.Hc, 42.50.Pq, 71.35.Pq

## I. INTRODUCTION

Cavity and quantum dot (QD) quantum electrodynamics has been studied with increasing interest over the past decade.[1,2] Refined spectroscopic methods, which allow the study of individual QDs, have been used to study the electronic structure of neutral and charged QDs. The ground state of a quantum dot which is charged by a single electron provides an approximate two-level system. Its excited state in form of a charged exciton $X^-$ (trion) has received special attention.[3–5] Spin-flip rates and decoherence mechanisms, as well as the fine-structure splitting of charged excitonic states in QDs have been explored in preparation for applications of QD systems in quantum information processing.[6–14]

When a QD or quantum well is put inside of a microcavity, the interaction strength between charge carriers and the cavity modes can be tuned when compared to the interaction with freely propagating light of the same frequency.[15] QD-filled cavities share a lot of similarities with cavities traversed by atomic beams but there are important differences.[2] QDs are usually held fixed relative to the mirror position. Their properties can be tailored by structuring and chemical composition but, at the same time, unwanted structural variations may occur. Their electronic degrees of freedom couple rather strongly to each other and to a background of lattice ions. This makes many-body effects important and decoherence times for charge-related degrees of freedom short, when compared to atoms. Spin-related phenomena, on the other hand, have considerably longer decoherence times due to the generally rather weak spin-orbit interaction and coupling to nuclear spins. Nevertheless, there are a lot of similarities. For example, the (heavy-hole) exciton provides an approximate representation of a two-level system.[16,17] This has made the spin degree of freedom in QDs of interest to realizations of qubits and for implementation of quantum information protocols.[14,18–20]

Recently, double-cavity systems have been proposed for entanglement generation at a distance.[21,22] Some important ground work has been accomplished by demonstration of reliable single electron spin-state preparation and state-dependent Faraday rotation for a single QD in experiment.[22,23] The basic idea is that a coherent light beam which is slightly detuned from an atomic or QD transition suffers a phase shift which depends on the initial state of the electronic system without significantly perturbing it, i.e., without real absorption. Consider, for example, a three-level $\Lambda$ system where, for some reason, the top level $|e\rangle$ interacts electromagnetically with state $|1\rangle$, but not with the ground state $|0\rangle$.[21] Hence, the phase shift of a nonresonant transmitted beam is sensitive to the population of state $|0\rangle$ and $|1\rangle$, in principle, allowing a quantum nondemolition measurement. Consider now a situation where such a nonresonant light beam interacts consecutively with two such identically prepared QD cavities. If one measures a phase shift for the transmitted light corresponding to one and only one QD in the electromagnetically active state $|1\rangle$, then lack of information regarding as to which of the two QDs was in state $|1\rangle$ has provided an entangled state between the physically remote QDs by this outcome of the measurement.

There are several potential problems with this scheme when applied to real QDs: Light may scatter or be absorbed on its way from the first to the second QD. Light, although nonresonant, may be absorbed by a QD which subsequently returns into its ground state by emitting a photon which reveals its initial state. Reflected light may be observed. Dissipative processes in the QDs modify the phase shift and may cause a decay of the initial state in which it was prepared, as well as the entangled state, once prepared. Unlike two atoms of the same species, two QDs are never perfectly alike. This leads to an asymmetry which tends to destroy entanglement because it makes possible, in principle, the identification of the QD which was responsible for the observed single-dot phase shift. Finally, phase is a continuous

 

variable. This leads to an uncertainty, as to whether the phase measurement really produces entanglement.

State-dependent phase shifts can be achieved by exploiting Pauli blocking and selection rules for optical excitation of electron-hole pairs in direct-gap semiconductors.[3,4,24] Consider a self-assembled III-V semiconductor QD with a single excess electron in the conduction-band ground state. In case that its spin is up, predominantly circularly polarized light of angular momentum $l_z=+1$ [positive helicity (+) corresponding to left circular polarization] interacts with the system, while circularly polarized light of angular momentum $l_z=-1$ [negative helicity (−) corresponding to right circular polarization] cannot due to angular momentum conservation and Pauli blocking when the initial state is a (predominantly) heavy-hole state of angular momentum $|3/2,\pm 3/2\rangle$.[22] Hence, circularly polarized light tuned below the trion transition suffers a phase shift depending on its helicity and the initial spin orientation of the excess electron.

An essential part of the game is to identify the phase shift arising from antiparallel spins, as compared to one arising from a parallel spin configuration, *without* revealing the identity of the spin, which caused it. In this paper we study how sensitively the transmitted light depends on the initial state in which the two remote excess electrons were prepared and to what extent information contained in the polarization dependence of the coherently transmitted light can reveal differences in the properties of the two quantum dot cavities. Of particular interest is to what extent an observed single-dot phase shift can reveal which of the two cavities was responsible for it. Technically, we study the transmission properties of a double quantum-dot-cavity system within time-independent scattering theory for a coherent nonresonant laser beam through a double quantum-dot-cavity system in a trion state. We use the elements of the single-cavity $S$ matrix to compute the $S$ matrix of the double cavity, i.e., reflection and transmission amplitudes. In particular, we address the effects of dissipation within the QDs and absorptive losses between the cavities leading to nonunitarity of the $S$ matrix. Moreover, we use the polarization dependence of the $S$ matrix elements to analyze the effects which arise from dissimilarities between the two cavities. The present study is limited to time scales ($\leqslant 0.1$ ns) at which unwanted spin-flip processes are negligible. Rather than studying a specific quantum dot cavity in detail, we use typical material parameters to estimate their effects upon the transmission amplitude. The paper is organized as follows. In Sec. II we introduce the model, outline the $S$-matrix approach, and give analytic results for single and double-cavity systems. In Sec. III we present numerical results and study properties of the transmitted light which reveal information about the double-cavity system. Summary and conclusions are given in Sec. IV.

## II. MODEL

### A. *S*-matrix approach

We consider a system consisting of two microcavities, each containing an InGaAs/GaAs self-assembled single QD, as illustrated schematically in Fig. 1 which also illustrates

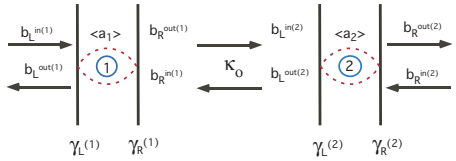


FIG. 1. (Color online) Schematic representation of the double-cavity system. $b_k^{l(i)}$ (with $k=L$, $R$, $l=$in, out, and $i=1,2$) denote the reservoir modes. $\langle a_i\rangle$ denotes the eigenmode of cavity $i=1,2$, indicated by the red dashed line. $\gamma_k^{(i)}$ entering Eq. (1) characterize the transparency of the cavity mirrors. $\kappa$ indicates the possibility of losses in the center reservoir. The dots with one excess electron are indicated by blue circles.

the notation used for the scattering states below. Each of the cavities contains a QD which is filled with one excess electron and, in the simplest case, shall be modeled as a four-level system to account for the lowest (trion) states: the degenerate ground state with the electron in the lowest conduction-band level with spin up or down, characterized by angular momentum $|1/2,\pm 1/2\rangle$, and two excited states with $J=\pm 3/2$, $|\pm 3/2\rangle$, for which the lowest conduction-band level is filled by two electrons of antiparallel spin and there is a single hole associated with a bulk $|3/2,\pm 3/2\rangle$ state. In the literature this state is termed the $X^-$ trion ground state. The transition between these two states will be called the trion transition. Effects from remote transitions are included also, as shall be discussed below. The cavity eigenmode is redshifted relative to the trion transition and is driven resonantly by external coherent laser light.

Since information on the initial state of the system may be obtained by analysis of single photon properties of the emitted light, we compute the photon $S$ matrix of this system. Its computation requires that one solves the coupled-light matter system in parallel. While the QD electrons couple to the cavity modes, the latter in turn couple to the light modes outside of the cavity via transparent mirrors, as sketched in Fig. 1. All three bath modes, $b_L$, $b_R$, and $b$, are assumed to have a spectrum which may be treated as continuous on an energy scale defined by the linewidth of the cavity eigenmodes. This condition, when applied to the central photon bath $b$, sets a lower limit to the distance between the two cavities. Following earlier work we employ the input-output formalism to describe the coupling between cavity modes and the three photon baths which are modeled as independent harmonic oscillators which couple linearly to the respective cavity modes, as sketched in Fig. 1.[25,26] Details of the Hamiltonian and a discussion of the derivation of the kinetic equations for the externally driven double-cavity eigenmode operators $a_j$ for cavity $j=1$ and 2 are given in the Appendix. Using the notation of Gardiner and Collett, they may be written as[25]

$$\dot{a}_j = \frac{1}{i\hbar}[a_j, H_j] - \frac{\gamma_L^{(j)} + \gamma_R^{(j)}}{2} a_j - \sqrt{\gamma_L^{(j)}}\, b_L^{in(j)} - \sqrt{\gamma_R^{(j)}}\, b_R^{in(j)} \quad (1)$$

and equivalently

$$\dot{a}_j = \frac{1}{i\hbar}[a_j, H_j] + \frac{\gamma_L^{(j)} + \gamma_R^{(j)}}{2} a_j - \sqrt{\gamma_L^{(j)}} b_L^{out(j)} - \sqrt{\gamma_R^{(j)}} b_R^{out(j)}. \tag{2}$$

Here $b_k^{in(j)}$ and $b_k^{out(j)}$, respectively, denote the photon field operators for incident (*in*) and outgoing (*out*) modes for cavity $j=1,2$ and "mirror" $k=L,R$. $H_j$ is the Hamiltonian for the isolated cavity resonator $j$, including the QD. In this formulation, the propagation of the light field is reduced to a temporal phenomenon, rather than a space- and time-dependent problem. The latter is restored when the photon field operators are put into the vector potential where the spatial shape of the modes, for example, plain waves, enters.

$$H_j = \hbar\omega_j a_j^\dagger a_j + \sum_\alpha \epsilon_{j\alpha} \psi_\alpha^{(j)\dagger} \psi_\alpha^{(j)} + H_j^{(D-a)}$$

denotes the Hamiltonian of cavity $j$. Next to the free Hamiltonian for the cavity mode $a_j$ it contains the free Hamiltonian of the dot, treated as an effective $N$-level system with single-particle operators $\psi_\alpha^{(j)}$. Note that these states are quasiparticle states of different numbers of constituent particles, whereby it is assumed that the energy levels $\epsilon_{j\alpha}$ are known. Denoting the QD states for the constituent electrons $e_n$ and for holes $h_n$, respectively, the ground state is a single-particle state $1e_1$ of spin state $\pm|1/2\rangle$ and the first excited state (across the main energy gap) is a three-particle state $2e_1 1h_1$ of spin $|\pm 3/2\rangle$.

The coupling between dot and light field $a_j$

$$H_j^{(D-a)} = \sum_{\alpha\beta} M_{(\alpha,\beta)}^{(j)} \psi_\alpha^{(j)\dagger} \psi_\beta^{(j)} a_j + \text{H.c.}$$

$M_{(\alpha,\beta)}^{(j)}$ denotes the dipole matrix element for a transition between pairs of trion levels $\alpha$ and $\beta$ in QD $j$. Note that they are polarization dependent. For example, levels $|1/2\rangle$ and $|3/2\rangle$ are coupled by $J=+1$ photons and levels $|-1/2\rangle$ and $|-3/2\rangle$ are coupled by $J=-1$ photons. The corresponding dipole matrix elements shall be termed $M_\pm^{(j)}$. Angular momentum nonconserving transitions between these four levels have an oscillator strength which is about 4 orders of magnitude smaller and are neglected.

The isolated ($I$) cavity mode including the QD evolves as

$$\dot{a}_j|_I = \frac{-i}{\hbar}[a_j, H_j] = -i\omega_j a_j - \frac{i}{\hbar}\sum_{\alpha\beta} M_{(\alpha,\beta)}^{(j)*} \psi_\beta^{(j)\dagger} \psi_\alpha^{(j)}. \tag{3}$$

Cavity mode and QD couple to each other via the interlevel polarization. In lowest order, frequency shifts enter additively for each trion transition $\alpha$-$\beta$. Since the $|1/2\rangle$–$|3/2\rangle$ transition drives the +1 polarization and the $|-1/2\rangle$–$|-3/2\rangle$ transition drives the −1 polarization contribution of $a_j$, treating $J=+1$ and $J=-1$ photon modes separately leads to two effective driven electronic two-level systems per QD. In order to determine $\psi_\beta^{(j)\dagger}(t)\psi_\alpha^{(j)}(t)$ entering Eq. (3), the time evolution of the latter must be computed in parallel to the kinetic equations for the light fields. The kinetic equations for the driven QDs are evaluated in lowest order in the dot-light-field coupling, which is rather weak, and by treating the cavity mode classically, i.e., by considering the laser light in a coherent state. Higher-order terms in the dot-light-field coupling, such as spontaneous emission, as well as other decay channels are treated phenomenologically within a Markov approximation and constant decay rates. This gives the kinetic equation of the QDs a Lindblad form.[27]

For all types of dissipators in the Lindblad equation which will be considered below, the effect of the polarization term in Eq. (3) is to make the cavity frequency complex, *i.e.* It leads to frequency-dependent renormalization and additional damping of the cavity field. Hence, it is convenient to solve the cavity mode equations via Fourier (or Laplace) transformation. As shown in the Appendix, elimination of the cavity mode from Eqs. (1) and (2) leads to a relation between input and output light field contributions and allows computation of the $S$-matrix elements for the individual and double quantum dot cavities.

Using the standard definition of the $S$ matrix via[28]

$$|i,out\rangle = S_{ij}|j,in\rangle \tag{4}$$

for in channels $|i,in\rangle$ and out channels $|i,out\rangle$ it takes the form

$$S(\omega) = \begin{pmatrix} r_1(\omega) & t_2(\omega) \\ t_1(\omega) & r_2(\omega) \end{pmatrix} \tag{5}$$

containing transmission and reflection amplitudes $r_l$ and $t_l (l=1,2)$.

Note that photon number conservation at a particular mirror $k=L,R$ of cavity $i$ requires[25,26]

$$\sqrt{\gamma_k^{(i)}} a_i = -b_k^{in(i)} + b_k^{out(i)}. \tag{6}$$

These relations help in the elimination of the cavity mode when establishing Eq. (4) for the present case, relating the output signal to a given input signal.

Due to the neglect of spin-flip processes and forbidden optical transitions, the $S$ matrix is diagonal in the circular left- and right-polarization bases. In this photon basis each trion acts, apart from remote transitions, like a two-level system and does not mix circular left- and right- polarization contributions. This becomes useful when treating the influence of the QDs entering via the electron polarization in Eq. (3) since only one pair of trion states couples to a specific circular polarization. Hence, it is most convenient to evaluate the $S$ matrix for the two circular polarization states independently. For the single quantum dot cavity $i$ and given circular polarization one obtains

$$S^{(i)}(\omega) = \begin{pmatrix} r_1^{(i)}(\omega) = \dfrac{\mathcal{N}_i(\omega) - \gamma_L^{(i)}}{\mathcal{N}_i(\omega)} & t_2^{(i)}(\omega) = -\dfrac{\sqrt{\gamma_L^{(i)}\gamma_R^{(i)}}}{\mathcal{N}_i(\omega)} \\ t_1^{(i)}(\omega) = -\dfrac{\sqrt{\gamma_L^{(i)}\gamma_R^{(i)}}}{\mathcal{N}_i(\omega)} & r_2^{(i)}(\omega) = \dfrac{\mathcal{N}_i(\omega) - \gamma_R^{(i)}}{\mathcal{N}_i(\omega)} \end{pmatrix}, \tag{7}$$

where $\mathcal{N}_j(\omega)=i(\tilde{\omega}_j-\omega)+\frac{\gamma_L^{(j)}+\gamma_R^{(j)}}{2}$ and $\tilde{\omega}_j$ denotes the effective (complex) cavity frequency renormalized by the presence of the QD. In general, it depends on frequency $\omega$, polarization, and intensity of the cavity mode. Unitarity of the $S$ matrix is readily shown for real $\tilde{\omega}_j$. Note also that we have adopted the notation of Ref. 25 rather than Ref. 26, which differ in the definition of the in-amplitude by a factor minus 1, leading to a relative minus sign between all corresponding $S$-matrix elements.

From reflection and transmission amplitudes of the single quantum dot cavity one obtains reflection and transmission amplitudes of the double quantum dot cavity by summing over all possible pathways arising from multiple reflections between the two inner mirrors, using $b_L^{in(1)}(t)=\kappa_o b_R^{out(2)}(t-t_{prop})$ and $b_R^{in(2)}(t)=\kappa_o b_L^{out(1)}(t-t_{prop})$. $t_{prop}$ denotes the time of flight between the two inside mirrors. Figure 1 sketches the situation. Light transmitted through the left cavity will suffer multiple reflections between the two inner mirrors according to the respective reflection amplitudes. Furthermore, photon loss between these two mirrors can be accounted for by a phenomenological transfer probability $0\leqslant\kappa_o\leqslant 1$ between the two inner mirrors, leading to a simple intercavity filter function $\kappa(\omega)=\kappa_o \exp\{i\omega t_{prop}\}$. A clean treatment of dispersive media has been offered in the literature and could, in principle, be implemented into this approach but goes beyond the scope of the present study.[29]

From this "sequential scattering" approach one obtains for the double quantum dot cavity

$$S(\omega)=\begin{pmatrix} r_1(\omega)=r_1^{(1)}(\omega)+\dfrac{t_1^{(1)}(\omega)\kappa(\omega)r_1^{(2)}(\omega)\kappa(\omega)t_2^{(1)}(\omega)}{1-\kappa(\omega)^2 r_2^{(1)}(\omega)r_1^{(2)}(\omega)} & t_2(\omega)=\dfrac{t_2^{(2)}(\omega)\kappa(\omega)t_2^{(1)}(\omega)}{1-\kappa(\omega)^2 r_2^{(1)}(\omega)r_1^{(2)}(\omega)} \\ t_1(\omega)=\dfrac{t_1^{(1)}(\omega)\kappa t_1^{(2)}(\omega)}{1-\kappa(\omega)^2 r_2^{(1)}(\omega)r_1^{(2)}(\omega)} & r_2(\omega)=r_2^{(2)}(\omega)+\dfrac{t_2^{(2)}(\omega)\kappa(\omega)r_2^{(1)}(\omega)\kappa(\omega)t_1^{(2)}(\omega)}{1-\kappa(\omega)^2 r_2^{(1)}(\omega)r_1^{(2)}(\omega)} \end{pmatrix}. \tag{8}$$

Note that by working with probability amplitudes quantum coherence between the two cavities is accounted for. This intuitive picture of multiple quantum pathways is easily generalized to multiple one- and two-sided cavity systems. In the Appendix we show that this result may also be obtained by treating the double quantum dot cavity as a single "scatterer." One obtains for the $S$ matrix

$$S(\omega)=\begin{pmatrix} \dfrac{(\mathcal{N}_1(\omega)-\gamma_L^{(1)})\mathcal{N}_2(\omega)+\kappa(\omega)^2(\mathcal{N}_2(\omega)-\gamma_L^{(2)})(\gamma_L^{(1)}+\gamma_R^{(1)}-\mathcal{N}_1(\omega))}{\mathcal{N}_1(\omega)\mathcal{N}_2(\omega)-\kappa(\omega)^2(\mathcal{N}_1(\omega)-\gamma_R^{(1)})(\mathcal{N}_2(\omega)-\gamma_L^{(2)})} & \dfrac{\kappa\sqrt{\gamma_L^{(1)}\gamma_R^{(1)}\gamma_L^{(2)}\gamma_R^{(2)}}}{\mathcal{N}_1(\omega)\mathcal{N}_2(\omega)-\kappa(\omega)^2(\mathcal{N}_1(\omega)-\gamma_R^{(1)})(\mathcal{N}_2(\omega)-\gamma_L^{(2)})} \\ \dfrac{\kappa\sqrt{\gamma_L^{(1)}\gamma_R^{(1)}\gamma_L^{(2)}\gamma_R^{(2)}}}{\mathcal{N}_1(\omega)\mathcal{N}_2(\omega)-\kappa(\omega)^2(\mathcal{N}_1(\omega)-\gamma_R^{(1)})(\mathcal{N}_2(\omega)-\gamma_L^{(2)})} & \dfrac{(\mathcal{N}_2(\omega)-\gamma_R^{(2)})\mathcal{N}_1(\omega)+\kappa(\omega)^2(\mathcal{N}_1(\omega)-\gamma_R^{(1)})(\gamma_L^{(2)}+\gamma_R^{(2)}-\mathcal{N}_2(\omega))}{\mathcal{N}_1(\omega)\mathcal{N}_2(\omega)-\kappa(\omega)^2(\mathcal{N}_1(\omega)-\gamma_R^{(1)})(\mathcal{N}_2(\omega)-\gamma_L^{(2)})} \end{pmatrix}. \tag{9}$$

Insertion of the single-cavity $S$-matrix elements (7) into Eq. (8) shows that both approaches yield identical results. For $\kappa_o=1$ and real effective cavity frequencies $\tilde{\omega}_j$ the $S$ matrices (7) and (9) are unitary. For the latter this can be shown, for example, by starting from expression (8), multiplying $S(\omega)$ by $\kappa(\omega)$, and combining each element $S_{lm}^{(i)}(\omega)$ with a factor $\kappa(\omega)$. Observing that multiplication by $\kappa(\omega)=\exp\{i\omega t_{prop}\}$ preserves unitary, unitary of Eq. (8) follows from unitarity of the single-cavity $S$ matrices.

The self-consistent mode occupancy in the cavities follows from Eq. (6) and the definition of reflection and transmission amplitudes

$$a_1(\omega)=\frac{1}{\sqrt{\gamma_L^{(1)}}}([r_1(\omega)-1]b_L^{in(1)}+t_2(\omega)b_R^{in(2)}) \tag{10}$$

and

$$a_2(\omega)=\frac{1}{\sqrt{\gamma_R^{(2)}}}([r_2(\omega)-1]b_R^{in(2)}+t_1(\omega)b_L^{in(1)}). \tag{11}$$

For the derivation of the results above we have assumed a specific helicity of the photon. For experiments using other input fields, such as linearly polarized light, transmission and reflection amplitudes are easily found from the contributions for helicities + and −. Considering light propagation along the $z$ axis, the relations between $x$ and $y$ components of the field to the circularly polarized components + and −

$$E_+=\tfrac{1}{\sqrt{2}}(E_x-iE_y),\quad E_-=\frac{1}{\sqrt{2}}(E_x+iE_y) \tag{12}$$

$$E_x=\tfrac{1}{\sqrt{2}}(E_++E_-),\quad E_y=\frac{i}{\sqrt{2}}(E_+-E_-) \tag{13}$$

readily give the $S$ matrix in the $x/y$ basis for direction index $j=1,2$

$$t_j^{xx}(\omega)=t_j^{yy}(\omega)=\tfrac{1}{2}(t_j^{++}(\omega)+t_j^{--}(\omega)), \tag{14}$$

$$t_j^{yx}(\omega)=-t_j^{xy}(\omega)=\tfrac{i}{2}(t_j^{++}(\omega)-t_j^{--}(\omega)), \tag{15}$$

$$r_j^{xx}(\omega) = r_j^{yy}(\omega) = \tfrac{1}{2}(r_j^{++}(\omega) + r_j^{--}(\omega)), \tag{16}$$

$$r_j^{yx}(\omega) = -r_j^{xy}(\omega) = \tfrac{i}{2}(r_j^{++}(\omega) - r_j^{--}(\omega)). \tag{17}$$

The pair of superscripts denotes polarization at exit and incidence, in this order. Inclusion of the polarization degree of freedom amounts to replacing scalar reflection and transmission amplitudes in Eq. (5) by $2\times 2$ matrices. Writing the $S$ matrix in the $x/y$ basis, for example, in Eq. (5) one makes the substitution

$$r_i \to \begin{pmatrix} r_i^{xx} & r_i^{xy} \\ r_i^{yx} & r_i^{yy} \end{pmatrix}, \quad t_i \to \begin{pmatrix} t_i^{xx} & t_i^{xy} \\ t_i^{yx} & t_i^{yy} \end{pmatrix},$$

for $i=1,2$. All the elements follow from Eq. (8), for specific $\pm$ polarization, and relations (14) and (17). Unitarity in the $S$ matrix (for empty cavities or filled cavities in absence of dissipation) leads to relations, such as

$$|r_1^{xx}|^2 + |r_1^{yx}|^2 + |t_1^{xx}|^2 + |t_1^{yx}|^2 = 1,$$

stating that incident $x$-polarized light can reemerge, reflected, or transmitted, as $x$- or $y$-polarized light. These $2\times 2$ blocks are diagonal in the $+/-$ polarization basis for the present system when trion spin-flip processes are neglected due to conservation of angular momentum and each trion transition couples to photons of one helicity only.

### B. Quantum dot dynamics

Using the helicity basis for the cavity modes and treating only transitions which conserve angular momentum, the driven quantum dot may be treated as a system of independent two-level systems. We consider three cases of QD dynamics to provide the polarization term which drives the cavity modes in Eq. (3): a fully coherent dynamics within the rotating-wave approximation, a pure dephasing (polarization decay) model based on the rotating-wave approximation solution, and a population and/or polarization decay model based on a Lindblad dissipator and Markovian elimination of the relative population. In all three cases, the kinetic equation for the electron density matrix equation can be written in Lindblad form[27]

$$\dot{\rho}_j = \frac{1}{i\hbar}[H_D^j, \rho_j] + \mathcal{L}\{\rho_j\}, \tag{18}$$

where

$$H_D^j = \sum_\alpha \epsilon_{j\alpha} \psi_\alpha^{(j)\dagger} \psi_\alpha^{(j)} + H_j^{(D-a)}$$

is the Hamiltonian for QD $j=1,2$, accounting for unitary evolution, and the dissipator is of the familiar form

$$\mathcal{L}\{\rho_j\} = \sum_\mu L_\mu^{(j)} \rho_j L_\mu^{(j)\dagger} - \frac{1}{2}\{L_\mu^{(j)\dagger} L_\mu^{(j)}, \rho_j\}$$

with $L_\mu^{(j)}$ denoting the Lindblad operators. For an $N$-level system, there are $N^2$ distinct Lindblad operators. They may be chosen as $L_\mu = \sqrt{\gamma_\mu}|i_\mu\rangle\langle j_\mu|$, with $i_\mu, j_\mu = 1,\ldots,N$. It is worth recalling the action of such an operator. For $i_\mu = j_\mu$ it provides pure dephasing (polarization decay) for every off-diagonal density matrix element $\rho_{i,j}$ containing the index $i_\mu$ with a rate $\gamma_\mu/2$. Lindblad operators $L_\mu = \sqrt{\gamma_\mu}|i_\mu\rangle\langle j_\mu|$, with $i_\mu \neq j_\mu$, lead to population decay for state $j_\mu$ and population increase for state $i_\mu$ at rate $\gamma_\mu$. Any off-diagonal element of $\rho$ containing the index $j_\mu$ decays at rate $\gamma_\mu/2$. These relations result from positivity conservation and have important consequences on coherence (entanglement) decay between two subsystems, even if there is no (further) direct interaction between them.

Since spin-flip processes, as well as angular-momentum–nonconserving transitions are neglected, the dynamics of the four-level trion system splits into two two-level systems when the cavity mode has given helicity $+/-$ 1. We shall assume driving of the cavities by coherent light of frequency $\omega$ and replace the photon operators by their expectation values $\phi^{(j)}(\omega) = \langle a_j(\omega)\rangle$. We consider moderate intensities such that detuning dominates the Rabi frequency. Thus only classical ("coherent") contributions in the electron-photon interaction are included in the Hamiltonian. However, spontaneous emission may be treated phenomenologically via Lindblad terms.

(i) *Coherent dynamics*. The simplest approach treats the dynamics in the QD without dissipation, i.e., $\mathcal{L}\{\rho_j\}=0$, and the coupling to the light field within the rotating-wave approximation. For constant cavity field amplitude and frequency $\omega$ the effective two-level system evolves unitarily under the propagator

$$U(t,0) = \exp\left\{\frac{i}{\hbar}(\epsilon_{j+} - \epsilon_{j-})\right\} \begin{pmatrix} \left[\cos(\Omega_j t) + \frac{\Delta_j}{i\hbar\Omega_j}\sin(\Omega_j t)\right]\exp\left\{-\frac{i\omega}{2}t\right\} & \frac{(\phi_o^{(j)} M_\pm^{(j)})}{i\hbar\Omega_j}\sin(\Omega_j t)\exp\left\{-\frac{i\omega}{2}t\right\} \\ \frac{(\phi_o^{(j)} M_\pm^{(j)})^*}{i\hbar\Omega_j}\sin(\Omega_j t)\exp\left\{\frac{i\omega}{2}t\right\} & \left[\cos(\Omega_j t) - \frac{\Delta_j}{i\hbar\Omega_j}\sin(\Omega_j t)\right]\exp\left\{\frac{i\omega}{2}t\right\} \end{pmatrix}. \tag{19}$$

Here $\epsilon_{j+}$ and $\epsilon_{j-}$ denote upper and lower trion states in QD $j$ (within a doublet which couples to light of given helicity), respectively. The expectation value of cavity mode $j$ is written as $\phi^{(j)}(t) = <a_j(t)> = \phi_o^{(j)} e^{-i\omega t}$.

$$\hbar\Omega_j = \sqrt{|M_\pm^{(j)}\phi_o^{(j)}|^2 + \Delta_j^2}$$

denotes the Rabi frequency for detuning $2\Delta_j$ between the trion transition and the cavity eigenmode. $M_\pm^{(j)}$ denotes the dipole matrix element for the transition within the doublet. Considering only initial states which are superposition states between spin-up and spin-down (ground) states in a given QD $j$, the time evolution of the electron polarization entering Eq. (3) for circular polarization of the cavity mode $\phi^{(j)}(t) = \langle a_j(t)\rangle = \phi_o^{(j)} e^{-i\omega t}$ is

$$\rho_{+-}^{(j)} \equiv \langle \psi_-^{(j)\dagger}\psi_+^{(j)}\rangle = \phi_j(t) M_\pm^{(j)} \left[ \frac{\sin 2\Omega_j t}{2i\hbar\Omega_j} - \frac{\Delta_j}{2\hbar^2\Omega_j^2}(1-\cos 2\Omega_j t)\right].$$

and the population of the upper trion state is

$$\rho_{++}^{(j)} \equiv \langle \psi_+^{(j)\dagger}\psi_+^{(j)}\rangle = \frac{|M_\pm^{(j)}\phi_o^{(j)}|^2}{(\hbar\Omega_j)^2}\sin^2\Omega_j t. \tag{20}$$

Hence the polarization response to driving with an electric field with frequency $\omega$ contains frequency components $\omega$, as well as contributions of frequency $\omega \pm 2\Omega_j$. These frequency side bands are related to population oscillations. Considering low intensities of the cavity modes and modest detuning (exceeding the linewidth of the transition), population oscillations may be neglected and the Rabi frequency is dominated by detuning. In this limit $\hbar\Omega_j \approx \Delta_j$ and

$$\rho_{+-}^{(j)} \approx a_j(t) M_\pm^{(j)} \frac{\exp\{-2i\Delta_j t\} - 1}{2\Delta_j},$$

this corresponds to neglecting the rapidly oscillation term $\exp\{-2i\Delta_j t\}$ against the $-1$ in the numerator. Furthermore, $\frac{|M_\pm^{(j)}\phi_0^{(j)}|}{\hbar\Omega_j} \ll 1$ suppresses population of the excited trion states and, herewith, spontaneous emission which reveals the initial state (*up or down*) of the individual QD. In summary, the polarization dependent frequency renormalization within this simple model leads to

$$\tilde{\omega}_j = \omega_j - \frac{|M_\pm^{(j)}|^2\Delta_j}{2\hbar^3\Omega_j^2}.$$

(i) *Pure dephasing model (polarization decay).* The case of weak dephasing is treated by inclusion of a Lindblad dissipator of the form (omitting the cavity index)

$$L_0 = \sqrt{\gamma_0}|+\rangle\langle +|,$$

where $|+\rangle$ denotes the trion state consisting of one heavy hole and an electron pair in the lowest conduction-band level $(e_1)$. $\gamma_0/2$ is the $+/-$ polarization decay rate. The Lindblad equation for $\rho_{+-}^{(j)}$ is solved in lowest order by inserting the coherent evolution for the populations, Eq. (20), and subsequent time integration. Again, neglecting frequency sidebands from population oscillations one obtains a revised complex effective cavity frequency from the pair of trion states which couples to the photons of specified helicity

$$\tilde{\omega}_j = \omega_j - \frac{|M_\pm^{(j)}|^2\Delta_j^2}{\hbar^3\Omega_j^2}\frac{1}{2\Delta_j - i\hbar\frac{\gamma_0^{(j)}}{2}}.$$

(iii) *Strong damping limit.* Finally we shall consider population and polarization decay from the trion state $|+\rangle$ into the corresponding ground state $|-\rangle$ and vice versa using

$$L_+ = \sqrt{\gamma_+}|-\rangle\langle +|, \quad L_- = \sqrt{\gamma_-}|+\rangle\langle -|.$$

Following the standard procedure of first solving for the polarization within the Markov approximation for the integral containing the population term and subsequent insertion of this result into the kinetic equations for the populations, one obtains a closed expression for the polarization.[30] Allowing transients which contain information about the initial population to decay, one is left with polarization contributions proportional to $\phi^{(j)}(t)$

$$\rho_{+-}^{(j)}(t) = \frac{(\gamma_-^{(j)} - \gamma_+^{(j)})}{(2\Gamma^{(j)} + \gamma_+^{(j)} + \gamma_-^{(j)})}\frac{iM_\pm^{(j)}\phi^{(j)}(t)}{i(\epsilon_{j+} - \epsilon_{j-} - \hbar\omega) + \hbar\gamma_0^{(j)}/2}$$

with intensity dependent

$$\Gamma^{(j)} = \frac{|M_\pm^{(j)}\phi^{(j)}|^2}{\hbar}\frac{\gamma_0^{(j)}}{(\hbar\gamma_0^{(j)})^2/4 + (\epsilon_{j+} - \epsilon_{j-} - \hbar\omega)^2}$$

and $\gamma_0^{(j)} \geqslant \gamma_+^{(j)} + \gamma_-^{(j)}$, whereby the equal sign holds when there are no additional pure dephasing contributions.

The populations are in dynamic equilibrium. In particular,

$$\rho_{--}^{(j)} \approx \frac{\Gamma^{(j)} + \gamma_+^{(j)}}{2\Gamma^{(j)} + \gamma_+^{(j)} + \gamma_-^{(j)}}.$$

The effective cavity frequency now is

$$\tilde{\omega}_j = \omega_j - \frac{|M_\pm^{(j)}|^2}{\hbar}\frac{(\gamma_-^{(j)} - \gamma_+^{(j)})}{(2\Gamma^{(j)} + \gamma_+^{(j)} + \gamma_-^{(j)})}\frac{1}{(\epsilon_{j+} - \epsilon_{j-} - \hbar\omega) - i\hbar\gamma_0^{(j)}/2}.$$

Within all three models the frequency shift depends on the occupancy of the cavity modes (10) and (11) and hence has to be computed self-consistently: the dot-induced frequency shift enters transmission and reflection amplitudes, which in turn influence the occupancy of the cavity mode. In the numerical examples below, where we are after Faraday rotation (quantum nondemolition measurement of the initial state of the double QD), detuning between resonator mode and trion transition dominates over mode population in the Rabi frequency by at least 2 orders of magnitude and hence this nonlinear effect is small.

### C. Effects from remote transitions

A (dissipative) two-level system is a rather simple model for a nonresonantly driven GaAs/InAs quantum dot. Equation (3) shows that every optically active transition, in principle, contributes to the renormalization of the frequency of

the cavity mode. Since the latter generally is chosen to be redshifted with respect to all transitions across the main energy gap of both QDs, they all lead to contributions of the same sign, whenever selection rules allow them. Details of the electronic properties of a QD strongly depend on its compositional and structural details. Therefore, we will account for remote transitions only in qualitative fashion to estimate their importance. The general formalism outlined here can readily be combined with a detailed electronic structure calculation which provides electronic transition energies and dipole matrix elements for a specific QD as input.

The contribution of a remote transition decreases inversely with detuning. Clearly a trade-off is called for. On one hand, the dominant phase shift contribution must arise from one (or more) transitions which is (are) sensitive to the spin orientation of the excess electron. This favors a small red detuning of the cavity mode relative to the main $X^-$ transition. On the other hand, sufficient detuning should be maintained to suppress absorption when the spin state of an individual electron should not be revealed by subsequent spontaneous emission.

The transition from the second (heavy-) hole level to the lowest electron level usually has a very small dipole matrix element and thus is not important.[31] While the top heavy-hole level(s) are dominated by the bulk $|3/2,\pm 3/2\rangle$ heavy-hole states due to strain in the QD, higher excited hole states may be dominated by the bulk $|3/2,\pm 1/2\rangle$ light hole, or even bulk $|1/2,\pm 1/2\rangle$ split-off-hole states.[32] For both of the latter, Pauli blocking and momentum conservation lead to phase shifts for the transition into the lowest electron level for a circularly polarized light when the transitions from the $|3/2,\pm 3/2\rangle$ heavy-hole state do not. Hence, if heavy-hole and light-hole transitions led to the same amount of a frequency shift, the spin state of the two excess electrons could not be determined. Three things help: light-hole associated levels will have typically 10–15 meV more detuning, their number will be small compared to heavy-hole associated levels, and the dipole matrix element for circularly polarized light between the cation $|s\rangle$ state and the $|3/2,\pm 1/2\rangle$ anion bulk light-hole state is a factor of $1/\sqrt{3}$ smaller than the one between cation $|s\rangle$ state and the $|3/2,\pm 3/2\rangle$ heavy-hole anion bulk state. In order to assess the effect from light-hole associated states we shall include a light-hole transition to the lowest electron conduction-band level in the numerical study below.

The lowest excited trion levels involving excited conduction-band states have been studied in detail both theoretically and experimentally.[5,6,8–10] In the absence of a magnetic field, they consist of Kramers-degenerate pairs of states grouped in a triplet of angular-momentum states $|\pm 5/2\rangle$, $|\pm 3/2\rangle$, and $|\pm 1/2\rangle$, corresponding to parallel alignment of the electron spins, and a higher-lying singlet of states $|\pm 3/2\rangle$ corresponding to antiparallel electron spins. Triplet and singlet are separated due to electron-electron exchange by typically 1–10 meV. Furthermore, the triplet is split via electron-hole exchange by typically 2 meV in CdSe/ZnSe QDs and $<1$ meV in InAs/GaAs QDS.[5,6,8–10] The triplet-singlet splitting (and to a lesser degree the triplet splitting) and optical selection rules lead to a spin-orientation sensitivity for circularly polarized light. For example, if originally the excess electron has spin up, the final state, after absorption of a photon of positive helicity, must be $|+3/2\rangle$, i.e., a singlet or a triplet state (each at half coupling strength), or $|-1/2\rangle$, i.e., a triplet state (at full coupling strength), for negative helicity of the photon. Essentially, the spin orientation of the excess electron defines a preferred direction leading to a polarization sensitive renormalization of the cavity mode without the need for Pauli blocking. Since the additional detuning of a heavy-hole associated level to these excited electronic states is on the order of 40 meV, this effect will be small.

## III. NUMERICAL ANALYSIS

Here we shall assume that the initial state of the two excess electrons (spin up or down) is known and evaluate properties of transmitted light by computation of the transmission amplitude $t_1^{ij}(\omega)$ for left incidence. This section consists of several parts. First we study the transmission spectrum of light as a function of polarization and initial trion-dot state for two identical QDs. The role of dissipation within and in between cavities, as well as remote transition effects, are analyzed. In the second part we discuss the effect of individual deviations from perfect identity between the two resonators, such as eigenmode detuning, differences in mirror, and QD properties, ending with a "worst case scenario" situation, in which several of these effects conspire to reveal the identity of the QD which has contributed to an observed phase shift and/or conceal the initial state of the two excess electrons altogether. By inspection of the transmission spectrum we shall identify laser pulse properties which optimize distinguishability between parallel and antiparallel spin configurations without revealing individual spin orientation. This is demonstrated by a time-dependent analysis of the pulse propagation.

The main material parameters which are the basis for this numerical study are listed in Table I. They are more or less of the order of magnitude which are characteristic for GaAs/InAs QD cavities which are currently under investigation.[22,23] Rather than specifying the intensity of the (left-)incident light beam, we specify the maximum electric field [for $r_1(\omega)=0$] in the left cavity. The chosen value is such that, for the chosen detuning, upper state populations still remains small (but noticeable). Any lower (more realistic) field strength would lead to practically identical results for $t_1^{ij}(\omega)$. The matrix element $M_\pm^{(j)}$ for the trion transition was estimated from the dipole matrix element between bulk $|s\rangle$ and $|p\rangle$ states and the relation between the energy contained in a classical electric field in the form of a sinusoidal standing wave and the one expressed in terms of cavity photons, using a dot radius of $D^{(j)}=15$ nm. Its value may be slightly larger (factor of 2–3) than what seems to have been achieved experimentally to date. The same value was used for remote transitions corrected, of course, according to selection rules. The decay rate $\gamma_+^{(i)}$ of the trion ground state $\epsilon_+^{(i)}$ was cautiously chosen somewhat high for InAs/GaAs QDs. $\gamma_-^{(i)}$ was set equal to zero. Also given in Table I is the energy chosen for a remote transition involving the first excited tripled state of the trion. The one for the transition involving

TABLE I. Quantum dot (QD) cavity parameters: cavity mode frequency $\omega^{(i)}$, cavity transmission rates $\gamma_L^{(i)}$ and $\gamma_R^{(i)}$, electric field amplitude $E_0^{(1)}$ in cavity 1, trion ground state energy $\epsilon_{3/2}^{(i)}=\epsilon_{-3/2}^{(i)}=\epsilon_+^{(i)}$, damping rates $\gamma_+^{(i)}$, $\gamma_0^{(i)}$, QD diameter $D^{(i)}$, energy of the remote transition involving the excited trion triplet state $\epsilon_r^{(i)}$, and associated damping rates $\gamma_r^{(i)}$ and $\gamma_{r0}^{(i)}$.

| Cavity $i$ | $\hbar\omega^{(i)}$ (eV) | $\hbar\gamma_L^{(i)}$ (meV) | $\hbar\gamma_R^{(i)}$ (meV) | $E_0^{(1)}$ (V/m) | $D^{(i)}$ (nm) | $M_\pm$ (meV) |
|---|---|---|---|---|---|---|
| 1 | 1.295 | 0.07 | 0.07 | $1\times10^7$ | 15 | 0.51 |
| 2 | 1.294 | 0.077 | 0.077 | | 15 | 0.49 |
| QD $i$ | $\epsilon_+^{(i)}$ (eV) | $\hbar\gamma_+^{(i)}$ (meV) | $\hbar\gamma_0^{(i)}$ (meV) | $\epsilon_r^{(i)}$ (eV) | $\hbar\gamma_r^{(i)}$ (meV) | $\hbar\gamma_{r0}^{(i)}$ (meV) |
| 1 | 1.300 | 0.05 | 0.05 | 1.340 | 0.2 | 0.2 |
| 2 | 1.301 | 0.05 | 0.05 | 1.340 | 0.2 | 0.2 |

the singlet is chosen to be 1.345 eV. The light propagation time between the two inner mirrors is chosen to be 50 ps for the present discussion.

Figures 2 and 3, respectively, show the magnitude and phase shift of the calculated transmission amplitude $t_1^{++}(\omega)$ for a symmetric double dot cavity system versus frequency as a function of initial population of the trion states spin up and down for incident light of positive helicity. Both cavities are identical, modeled with the parameters of cavity 1 and QD 1 in Table I. In this calculation the Markovian population decay model has been used. Remote band effects contain a transition between a light-hole associated trion transition detuned from resonance by 15 meV and a heavy-hole transition into the first excited electron levels consisting of a triplet and singlet, as discussed above. It can be seen in Fig. 2 that the interplay between the two cavities (solid and dashed lines) leads to an intricate Fabry-Pérot-like transmission spectrum superimposed upon the single-cavity resonance (dotted line). Depending on the initial spin pair state, the resonance frequency of the double cavity is lowered relative to its "empty" value (dashed curve) due to the redshifted detuning of the cavity mode relative to the trion transition. For a single (empty) cavity it can be seen that the linewidth is larger by a factor of 2 and the resonance lacks the fine structure imposed by interference between the two cavities. A single cavity (dotted line for the single empty cavity) shows a single peak for given spin orientation, with a Stark shift dependent upon spin orientation. For the filled double cavity there are three transmission spectra corresponding to both spins up, both spins down, and one spin up-one spin down (antiparallel spin orientation). Since both cavities are perfectly identical, the results for the latter case are indistinguishable. It can be seen that neither are phase shifts from the individual cavities perfectly additive, nor do the maxima occur at exactly the same photon energy due to the spin-orientation dependence of the frequency renormalization (Stark shift). It should be pointed out that for antiparallel spins the two cavities are slightly off resonance to one another. This causes enhanced multiple reflections of light between the cavities and the buildup of new resonances leading to a transmission spectrum which differs from the one for parallel spin orientation not only in energy position (Stark shift) but also in shape: When the spins in both cavities are parallel the now truly identical cavities are at resonance with one another. Then the two transmission amplitudes are frequency shifted and distorted nonlinearly relative to each

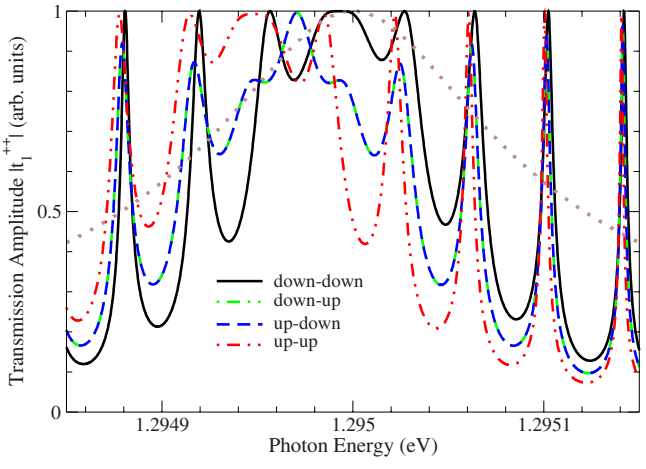


FIG. 2. (Color online) Absolute value of the transmission amplitude for left-circular polarized incident light as a function of photon energy and spin orientation for the double- and single-cavity systems. Solid and (dot-)dashed lines are for the double-cavity system. The dotted line is for the empty single left cavity.

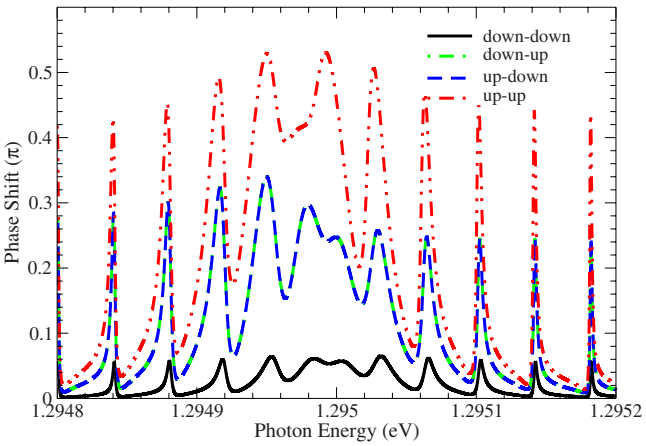


FIG. 3. (Color online) Phase shift (relative to the empty double cavity) for left-circular polarized incident light as a function of photon energy and spin orientation. The orange solid line shows the pulse with of a 0.2 ns Gaussian pulse for reference.

other near the main resonance peak. Figures 2 and 3 identify optimal driving frequencies and pulse duration for the incident laser field which optimize transparency and distinguishability of parallel and antiparallel spin directions.

The light-hole transition, with selection rules "opposite" to those for heavy-hole trion transitions, which was included into the model is responsible for the nonzero relative phase shift for the "down-down" spin configuration in Fig. 3 (solid line). Figure 2 shows that, comparing the peak position of the solid line versus that of the dotted line, for the present detuning of 5 meV the frequency renormalization due to remote transitions is small. It is about equal for the light-hole transition and the combined effect from the triplet and/or singlet associated transition of $X^-$. The spin-orientation dependence from the latter is found to be insignificant and cannot be resolved on the scale of Figs. 2 and 3.

Due to the relatively large detuning (compared to linewidth and light intensity) dissipation (decoherence) within the QDs plays a minor role and the maximum transmission probability still lies around 97% for up-down and around 94% for up-up initial configuration, which can hardly be resolved in Fig. 2. Virtually identical results are obtained within the pure dephasing model indication that polarization decay is mainly responsible for the slight reduction in transmittivity. Moreover, the phase shifts (relative to empty cavities) obtained are practically identical for all three models for the dot dynamics presented above. Generally, the pure dephasing model and the population decay model, although quite different in spirit, give identical results for moderate to large detuning. For small to zero detuning, however, where significant population of the upper trion level occurs, the three models for the QD dynamics differ significantly, as has to be expected. Off resonance, the dominant linewidth contribution is due to mirror properties.

A similar picture unfolds for the reflection amplitude $r^{++}(\omega)$ (not shown here) which has dips and suffers a phase shift at frequency-shifted resonances, dependent upon relative spin orientation. $t_i^{--}(\omega)$ and $t_i^{++}(\omega)$, as well as $r_i^{--}(\omega)$ and $r_i^{++}(\omega)$ show perfect symmetry with respect to simultaneous spin flips.

A very useful quantity to study differences in spin-pair configuration and structural properties of the two cavities is $t_1^{yx}(\omega)$ which gives the probability amplitude for left-incident linear $x$-polarized light to emerge at the other end as linear $y$-polarized light (Faraday rotation), as evident from Eq. (15). For identical cavities it is zero for antiparallel spins due to Kramers degeneracy (time-reversal symmetry in the absence of a magnetic field), and nonzero for parallel spins, the latter, however, only if there is spin sensitivity. The real part of $t_1^{yx}(\omega)$ (quadrature) for the two identical cavities is shown in Fig. 4. While the quadrature is zero for antiparallel spins one observes a multipeak structure for parallel spin orientation. The latter corresponds to the peaks for parallel spin orientation in Fig. 2. Note that, regardless of the action of remote transitions and their selection rules, $t_1^{yx}(\omega)=0$ for antiparallel spins, as long as the two cavities are identical. Remote transitions with selection rules opposite to those of the primary heavy-hole trion transition merely reduce signal strength and the problem becomes rather how to interpret a

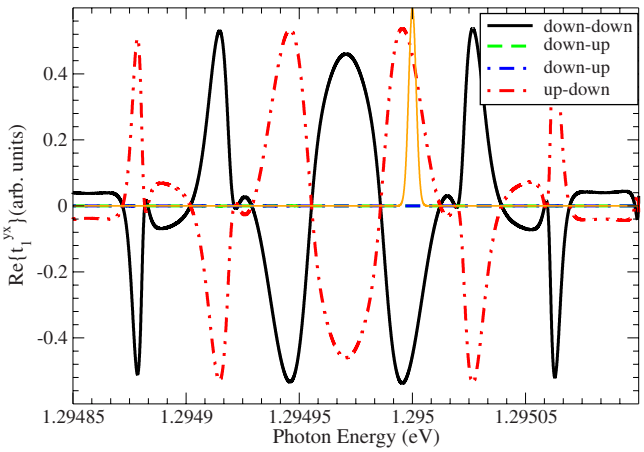


FIG. 4. (Color online) Real part of the transmission amplitude $t_1^{yx}$ for $x$-polarized incident light as a function of photon energy and spin orientation for the double- and single-cavity systems. Solid, dashed, and dot-dashed lines are for the double-cavity system; dotted lines are for the single cavity.

small value for a measured phase shift. For reference in Fig. 4 we also give the spectral shape of a Gaussian laser field of central photon energy 1.295 eV and a duration of 0.2 ns. It can be seen that careful choice of the former allows optimization of the signal-to-noise ratio in the quadrature measurement which will be utilized below to offset adverse effects from nonidentical scatterers.

Even though the two cavities may be perfectly identical, light scattered along its way between the two cavities may reveal whether a phase shift occurred already in the first cavity or not. Scattering in the region between cavities becomes the dominant loss mechanism when the qubit separation is increased.[21] Moreover, when the two qubits are not identical, for example, when the spins are antiparallel to each other and/or due to unwanted structural imperfections, multiple reflections between the cavities are needed to establish the resonances of the double-cavity system. In this case, even a small scattering probability for a single run may lead to essential losses in the transmitted signal, as well as a loss in the change of the phase angle. To illustrate this point we consider a double-cavity system as above; however, the eigenfrequency of the left (empty) cavity is 1.294 meV instead of 1.295 meV. The absorption amplitude is $\kappa_0=0.99$. Magnitude and phase shift of the calculated transmission signal $t_1^+(\omega)$ are given, respectively, in Figs. 5 and 6. Figure 5 also shows the transmission amplitudes for the left and right (empty) cavities (dotted lines). A significant reduction in the transmitted signal, as well for the phase shift, is apparent in the region between the single-cavity resonances. In the absence of losses the transmission amplitude should reach "one" near the center between the single-cavity resonances. Closer inspection of Figs. 5 and 6 shows that the up-down and down-up signals are no longer identical: the spin up-down configuration further detunes the two cavities and dissipative effects are enhanced, while the spin down-up configuration reduces detuning over the one for parallel spins. The global features of the real part of $t_1^{yx}(\omega)$ are shown in Fig. 7. Close inspection of the resonances reveals an anti-

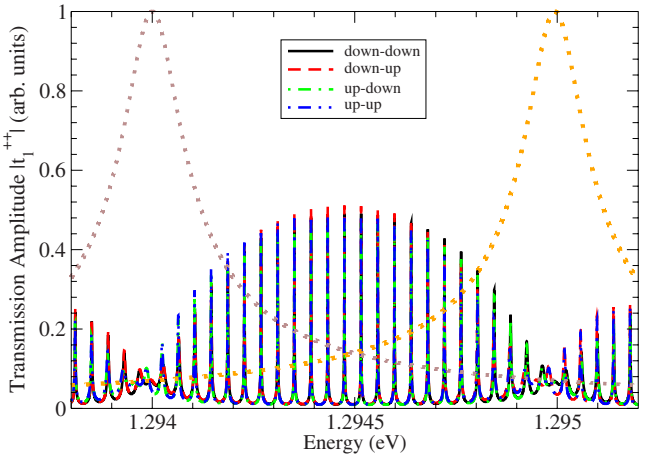


FIG. 5. (Color online) Absolute value of the transmission amplitude for left-circular polarized incident light as a function of photon energy and spin orientation in the double- and single-cavity systems. Detuning of the left cavity relative to the right cavity is −1 meV and $\kappa$=0.99. Narrow resonances in the center [solid (down-down), dashed (down-up), dot-dashed (up-down), and double-dot-dashed (up-up) lines] are for the double-cavity system; and wide resonances (dotted lines) are for the single cavities.

symmetry with respect to simultaneous spin flips, as well as the fact that the $y$ component of the transmitted light is no longer zero for antiparallel spins, especially, near the single-cavity resonances. However, for the resonances near the center between the single-cavity resonances (around 1.2945 eV) have small signal for antiparallel spin orientation. The amplitude for parallel spin is reduced to about 25% of the one for the case for identical cavities, Fig. 4. In principle, $t_1^{yx}(\omega)$ allows distinction between the two antiparallel configurations once the structural properties of the cavity are known. This distinguishability is optimized for laser center frequencies close to the single-cavity resonances, while center frequencies placed on one of the peaks about halfway between

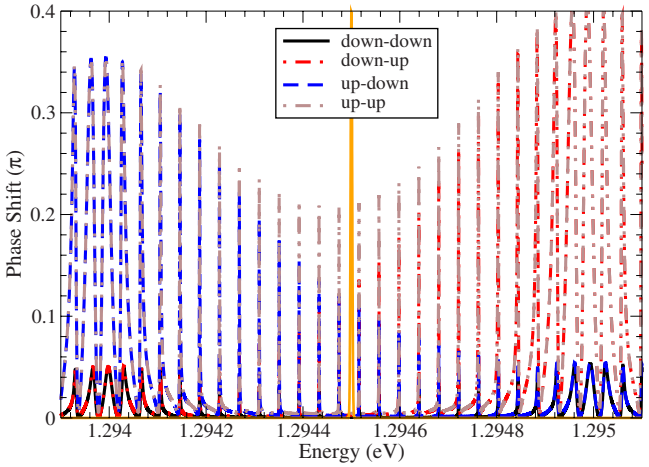


FIG. 6. (Color online) Phase shift (relative to empty cavities) for left-circular polarized incident light as a function of photon energy and spin orientation in the quantum dots. Detuning (left cavity) is −1 meV and $\kappa_0$=0.99, as for Fig. 5.

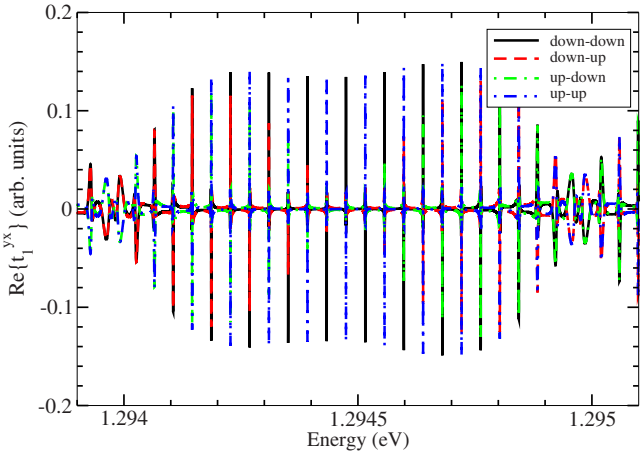


FIG. 7. (Color online) Real part of the transmission amplitude $t_1^{yx}$ for $x$-polarized incident light as a function of photon energy and spin orientation in double- and single-cavity systems. Detuning is −1 meV and $\kappa_0$=0.99, as for Fig. 5.

the single-cavity resonances optimizes distinguishability between parallel and antiparallel spin orientations, while masking the individual spin orientation. Figures 5 and 6 should give the global features near the cavity resonances. Below we shall zoom in to explore and utilize spectral details.

We now consider the effects from differences in structural properties of the two cavities *individually*: mirror reflectivities [$\gamma_L^{(1)}=\gamma_R^{(1)}=0.077$ meV, $\gamma_L^{(2)}=\gamma_R^{(2)}=0.077$ meV, absorption between the cavities $\kappa$=0.98 (without detuning), a trion transition energy in the left cavity of 1.301 eV, a maximum light field in the left cavity of $10^8$ V/m, and the right QD shifted by 5% of the cavity wavelength away from maximum intensity (corresponding to $M_\pm^{(2)}$=0.49 meV instead of $M_\pm^{(1)}$=0.51 meV]. Results for the real part of $t_1^{yx}(\omega)$ for down-up spin orientation are shown in Fig. 8.

For the variations chosen here, effects from $\kappa_0$ are of order $10^{-4}$ and cannot be resolved on the scale used in Fig. 8. The effect for $E_0=10^8$ V/m $10^{-3}$ is of order $10^{-3}$ and marks the onset of intensity dependence (nonlinearities) via the Rabi frequency, absorption, and excitation into the trion ground state. The remaining effects studied can be seen to be of the order of $\leqslant 10^{-1}$. For example, a variation of the main trion transition by 1 meV, which is quite realistic, and a nominal detuning of about 5 meV lead to a significant effect. Clearly, the smaller the detuning from the trion transition is chosen, the more seriously small variations between cavity properties will be revealed. On the other hand, large detuning will bring remote effects into play.

Finally, we consider a worst case scenario in which different effects conspire to allow identification of the up-down initial state against the down-up state or the spin orientation altogether, when only a small (unfavorably chosen) energy window is inspected. We consider a double cavity in which the right cavity has the structural parameters of system 1 in Table I, and the left dot has the parameters of system 2. Again we use the real part of $t_1^{yx}(\omega)$ to characterize the double-cavity system and show numerical results in Fig. 9. Mapping out a sufficiently wide energy region around the

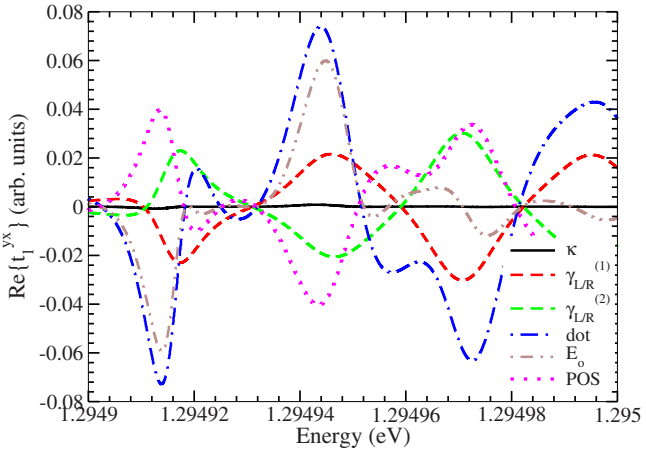


FIG. 8. (Color online) Real part of the transmission amplitude $t_1^{yx}$ for *down-up* spin orientation and *x*-polarized incident light as a function of photon energy in the double-cavity system. We consider individual deviations from the parameters of cavity and QD "1" in Table I which are listed under cavity and QD "2": $\kappa=0.98$, $\gamma_L^1=\gamma_R^1=0.077$ meV, $\gamma_L^2=\gamma_R^2=0.077$ meV, $\epsilon_+^{(1)}=1.301$ meV, $E_0=10^8$ V/m, and $M_\pm=0.98$ meV. Effects from $\kappa_0$ and $E_0$ cannot be resolved on this scale.

systems resonances, particularly near the position of single-cavity resonances, allows identification of single spin orientations (see Fig. 7). However, based on the lesson learned from detuned cavities above we zoom in and select among the central resonance peaks the one with optimal distinguishability between relative spin orientations. Shown in the figure is also the spectral line shape of a 0.2 ns Gaussian pulse (dotted line). We observe that the maximal signal is about 0.1 for parallel spins and 0.02 for antiparallel spins. Unlike for sole cavity detuning and intercavity losses there is a clear asymmetry across the resonance. In particular, the zero for antiparallel spins no longer coincides with the maximum (minimum) for parallel spins. However, this is not too problematic since even relatively long pulses average over the resonance. Hence to minimize distinction between the up-

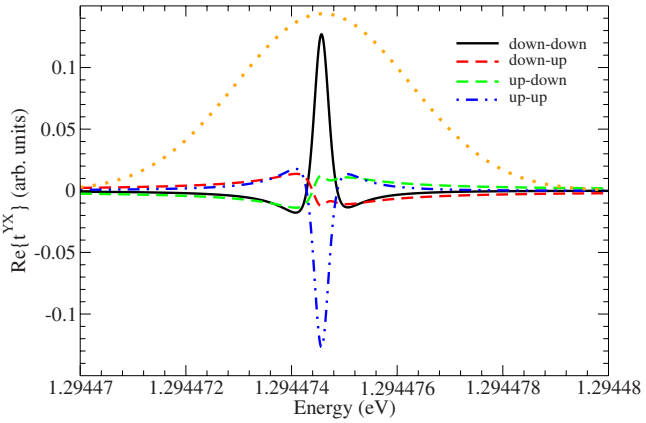


FIG. 9. (Color online) Real part of the transmission amplitude $t_1^{yx}$ for *x*-polarized incident light as a function of photon energy and spin orientation in the asymmetric double-cavity system. Structural parameters are given in Table I and the main text.

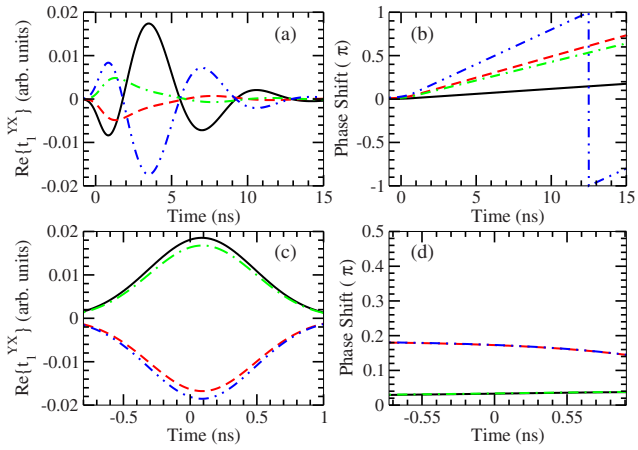


FIG. 10. (Color online) [(a) and (c)] Real part of the transmission amplitude $t_1^{yx}$ for *x*-polarized incident light as a function time and spin orientation in the asymmetric double-cavity system, respectively, for pulse center frequencies of 1.294 474 and 1.295 000 eV. [(b) and (c)] Phase shift (relative to empty cavities) for left-circular polarized incident light of pulse center frequencies 1.294 474 and 1.295 000 eV, respectively. In both cases the incident Gaussian pulse has a duration of 0.2 ns. Note the different time scale for rows 1 and 2. Solid black lines for down-down, dashed red lines for down-up, dash-dotted green lines for up-down, and dash-double-dotted blue lines for up-up spin orientation, respectively. Structural parameters are given in Table I and the main text.

down and down-up configurations while obtaining a good signal one would have to probe the system by sufficiently long pulses with central photon energy near the zero of $t_1^{yx}(\omega)$, at 1.294 474 meV in the present example. Note that for this strategy to succeed one needs to have accurate control of the center frequency and very low intercavity losses.

In order to test this strategy we consider an incident 0.2 ns Gaussian laser pulse of center frequency 1.294 474 meV and study the time evolution of quadrature $\mathrm{Re}\{t_1^{yx}(t)\}$ and phase shift for the transmitted signal versus spin orientation in Figs. 10(a) and 10(b). The time of arrival of the peak of the incident pulse is set equal to zero. The temporal evolution of the envelope of $\mathrm{Re}\{t_1^{yx}(t)\}$ shows that, due to the two nonresonant scatterers which build up the resonance which we selected, light partially gets trapped between the cavities and emerges in an oscillatory fashion on the right with considerable time delay. Transmittivity is quite low at a few $10^{-4}$; however, the transmitted signal for antiparallel spin is clearly suppressed compared to parallel spin polarization. Moreover, due to the prolonged stay of the pulse within the double-cavity system the effective coupling between light and quantum dot is enhanced and leads to a phase shift which is larger than for identical cavities since it grows linearly in time. In principle, observation of the slope of the phase shift could be used to reveal spin flips induced, for example, by the interaction with nuclear spins.

For comparison, Figs. 10(c) and 10(d), respectively, shows quadrature $\mathrm{Re}\{t_1^{yx}(t)\}$ and phase shift for a 0.2 ns pulse of center frequency 1.295 000 eV. In this case the transmission is sensitive to the spin orientation of the right dot, while the spin orientation on the left dot (with the 1.294 eV empty

cavity eigenmode) is largely concealed. Moreover, the pulse quickly passes through the double-cavity system leading to a simple pulse shape and comparatively small phase shifts.

The pulse shape of the transmitted light reflects the spectral regime of the incident pulse: pulses which drive resonances associated predominantly with a single-cavity pass through the double cavity relatively quickly on a time scale $t_{prop}$. Pulses which drive Fabry-Pérot--like resonances may spend a considerably longer time within the double cavity. Increasing $t_{prop}$, i.e., increasing the distance between the two cavities, relative to the pulse duration decreases the separation of Fabry-Pérot resonances and, hence, the ability to drive them individually. Therewith, spin sensitivity is lost, since for adjacent resonances the sign of the quadrature for given parallel spin orientation oscillates. Moreover, increasing the distance of separation will increase photon loss.

## IV. SUMMARY AND CONCLUSIONS

In summary we have presented a self-consistent scattering approach for the interaction between a coherent light beam and a double-cavity system. Each cavity contains a single quantum dot which, in turn, is charged by a single excess electron. Expressions for the frequency-dependent $S$ matrix have been derived for circular and linear light polarizations. The dynamics of the nonresonantly driven trion transitions has been accounted for three cases of dissipation within the dot: no dissipation, pure dephasing, and population decay. Spin-flip processes have been ignored which implies that the present work has relevance only for time scales below intrinsic spin-flip times (typically $\approx 1$ ns). In view of its relevance to entanglement formation at a distance, we have used these results for a numerical analysis of the influence of structural properties of the cavity system on the transmitted light. In particular, the effects from dissipation and asymmetries in the double-cavity system on the polarization dependent transmission coefficients have been investigated.

Dissipative effects within the QD have been found to be of minor importance as long as detuning of the cavity mode dominates over (i) the linewidth broadening due to effects, such as spontaneous emission and charge fluctuations, and (ii) over light intensity in the Rabi frequency.

Phase shift and polarization dependence of the transmission amplitude have been found to be a sensitive means to determine the initial spin-pair state of the two excess electrons, but also for dissimilarities in the two cavities. The transmission spectrum of the double cavity can be interpreted as a hybridization of the resonances of the individual cavities and Fabry-Pérot resonances established between the two cavities. It has been shown that different frequency regimes give complementary information about relative and individual spin orientation. This can be used to select and optimize input pulses for specific tasks.

A severe degradation of the transmitted signal has been found when detuning of the cavity modes conspires with just small dissipative losses of light between the two cavities. This can be understood by interpreting the double-cavity resonances as arising from multiple reflections at the two inner mirrors as in a Fabry-Pérot interferometer. Furthermore, with decreasing detuning from the trion transition variations in QD and cavity, including the coupling between cavity mode and QD, gain in importance.

Remote transitions involving empty electron Kramers doublets have a measurable contribution to total phase shifts; however, it is basically independent from the initial spin orientation of the excess electrons. Due to the large detuning of remote transitions to the cavity mode any fine-structure splitting of remote levels of the order of a few meV does not lead to significant effects. Light-hole level associated trion transitions display spin sensitivity which is opposite to that of heavy-hole associated transitions. While they add spin-orientation dependence to the output, and thus modify relative phase shifts for the various spin orientations, as well as the quadratures for parallel spins, they directly do not seriously hurt entanglement generation into an antiparallel spin Bell state by measurement "$t_1^{yx}=0$," as long as cavities are identical. For dissimilar cavities, inspection of the quadrature of the transmission coefficient $t_1^{yx}$ allows the identification of the optimal pulse duration and central frequency for the input pulse, such that measurement $t_1^{yx}=0$ implies, after proper initial state preparation of the electron spins, projection upon a Bell state. These parameters have to be determined from measurement and/or a calculation involving the details of the particular double cavity at hand.

The present study has concentrated on the transmission properties of a two-sided double-cavity system. In fact, equivalent information is contained in the reflection coefficients. This has to be considered when attempting entanglement generation at a distance. For this reason, one-sided cavities may be advantageous for this task, as has been discussed elsewhere.[34] The present approach is readily extended to a more detailed inclusion of the QD electronic structure, applied magnetic fields, other cavity types, as well as larger cavity arrays.[35]

## ACKNOWLEDGMENTS

The author wishes to acknowledge helpful discussions with J. Grond and U. Hohenester.

## APPENDIX: INPUT-OUTPUT APPROACH FOR A DOUBLE-CAVITY SYSTEM

The Hamiltonian of the double-cavity system sketched in Fig. 1 is written as

$$H = \sum_{i=1,2} (H_i + H_{i-B}) + H_B.$$

$H_i$ are the Hamiltonians for the two quantum dot (QD) cavities $i=1,2$. The bath Hamiltonian

$$H_B = \sum_{k=L,C,R} H_k$$

consists of the contribution from the region to the left ($L$), to the right ($R$), and from the central region between the two cavities ($C$). They have a continuous spectrum and are of the generic form[25,26]

$$H_k = \int_{-\infty}^{+\infty} d\omega \hbar\omega b_k^\dagger(\omega) b_k(\omega).$$

The interaction contributions $H_{i-B}=\Sigma_k H_{i-k}$ are of the form

$$H_{i-k} = -i\hbar \int_{-\infty}^{+\infty} d\omega \kappa_{i-k}[a_i^\dagger b_k(\omega) - b_k^\dagger(\omega) a_i].$$

Note that an explicit spectral density has been omitted and the lower integration boundary has been set to $-\infty$.[25,26] A physical justification for the latter has been given in the literature. The spectral density can be absorbed into the definition of the bath operators $b_k$ and $b_k^\dagger$ and, eventually, in the effective coupling constants between bath and cavity mode $\gamma_l^{(i)}$ as shown in Fig. 1.

The resulting equations of motion for the photon modes are

$$\dot{b}_L(\omega) = -i\omega b_L(\omega) + \kappa_{1-L}(\omega) a_1,$$

$$\dot{a}_1 = -i/\hbar[a_1, H_1] - \int_{-\infty}^{+\infty} d\omega \kappa_{1-L}(\omega) b_L(\omega) - \int_{-\infty}^{+\infty} d\omega \kappa_{1-C}(\omega) b(\omega),$$

$$\dot{b}(\omega) = -i\omega b(\omega) + \kappa_{1-C}(\omega) a_1 + \kappa_{2-C}(\omega) a_2,$$

$$\dot{a}_2 = -i/\hbar[a_2, H_2] - \int_{-\infty}^{+\infty} d\omega \kappa_{2-C}(\omega) b(\omega) - \int_{-\infty}^{+\infty} d\omega \kappa_{2-R}(\omega) b_R(\omega),$$

$$\dot{b}_R(\omega) = -i\omega b_R(\omega) + \kappa_{2-R}(\omega) a_2,$$

where we have set $b_C(\omega)=b(\omega)$ and will, from now on, omit the index $C$ for the central region bath modes, for simplicity of notation.

Feeding the formal solutions (retarded or advanced) for the bath modes into the equations for $a_i$ and making the assumption that the bath-cavity-mode couplings are frequency independent over the frequency regime in the vicinity of the cavity resonances, one obtains

$$\dot{a}_1 = \frac{-i}{\hbar}[a_1, H_1] - \frac{\gamma_L^{(1)} + \gamma_R^{(1)}}{2} a_1 - \sqrt{\gamma_L^{(1)}} b_L^{in} - \sqrt{\gamma_R^{(1)}} b^{in} - \frac{\sqrt{\gamma_R^{(1)} \gamma_L^{(2)}}}{2} a_2 \tag{A1}$$

and

$$\dot{a}_2 = \frac{-i}{\hbar}[a_2, H_2] - \frac{\gamma_L^{(2)} + \gamma_R^{(2)}}{2} a_2 - \sqrt{\gamma_R^{(2)}} b_R^{in} - \sqrt{\gamma_L^{(2)}} b^{in} - \frac{\sqrt{\gamma_R^{(1)} \gamma_L^{(2)}}}{2} a_1. \tag{A2}$$

The effective coupling constants are $\gamma_L^{(1)}=2\pi g_L(\omega)\kappa(\omega)_{1-L}^2$, $\gamma_R^{(1)}=2\pi g(\omega)\kappa(\omega)_{1-C}^2$, $\gamma_L^{(2)}=2\pi g_C(\omega)\kappa(\omega)_{2-C}^2$, and $\gamma_R^{(2)}=2\pi g_R(\omega)\kappa(\omega)_{2-R}^2$, where we have indicated how to accommodate the density of states $g_k(\omega)$ (set equal to one in the definition of the bath Hamiltonians above) in these definitions. These two equations have been obtained with the retarded solutions for the photon bath fields. The bath *in* fields are defined as $(g_k(\omega)=1)$

$$b_k^{in}(t,t_0) = \frac{1}{\sqrt{2\pi}} \int_{-\infty}^{+\infty} d\omega e^{-i\omega(t-t_0)} b_k^0(\omega)$$

for some time $t_0<t$ in the distant past when the incident photon wave packet has not yet interacted with the cavities in the spirit of time-dependent scattering theory.[33] Using the advanced solutions an equivalent set of differential equations may be found,

$$\dot{a}_1 = \frac{-i}{\hbar}[a_1, H_1] + \frac{\gamma_L^{(1)} + \gamma_R^{(1)}}{2} a_1 - \sqrt{\gamma_L^{(1)}} b_L^{out} - \sqrt{\gamma_R^{(1)}} b^{out} + \frac{\sqrt{\gamma_R^{(1)} \gamma_L^{(2)}}}{2} a_2 \tag{A3}$$

and

$$\dot{a}_2 = \frac{-i}{\hbar}[a_2, H_2] + \frac{\gamma_L^{(2)} + \gamma_R^{(2)}}{2} a_2 - \sqrt{\gamma_R^{(2)}} b_R^{out} - \sqrt{\gamma_L^{(2)}} b^{out} + \frac{\sqrt{\gamma_R^{(1)} \gamma_L^{(2)}}}{2} a_1, \tag{A4}$$

which contain the bath *out* fields

$$b_k^{out}(t,t_1) = \frac{1}{\sqrt{2\pi}} \int_{-\infty}^{+\infty} d\omega e^{-i\omega(t-t_1)} b_k^1(\omega)$$

for some time $t_1>t$ in the distant future when the photon wave packet has ceased to interact with the cavities. Frequency integration of retarded and advanced integral solutions for the bath modes yields the relations

$$b_L^{out} - b_L^{in} = \sqrt{\gamma_L^{(1)}} a_1, \tag{A5}$$

$$b_R^{out} - b_R^{in} = \sqrt{\gamma_R^{(2)}} a_2, \tag{A6}$$

and

$$b^{out} - b^{in} = \sqrt{\gamma_R^{(1)}} a_1 + \sqrt{\gamma_L^{(2)}} a_2. \tag{A7}$$

Note that the central bath modes are fed by both cavities. In turn, inspection of Eqs. (A1) and (A3) shows that the cavity field $a_1$ is driven by $b_L$, $b$, and $a_2$. Similarly, the cavity field $a_2$ is driven by $b_R$, $b$, and $a_1$. Comparison of Eqs. (A1)–(A4) with those for single double-sided cavities Eqs. (1) and (2) leads to the following identification of the *in* and *out* fields

associated with the inside mirrors $1R$ and $2L$:

$$b_R^{in(1)} = b^{in} + \frac{\sqrt{\gamma_L^{(2)}}}{2} a_2 \tag{A8}$$

and

$$b_L^{in(2)} = b^{in} + \frac{\sqrt{\gamma_R^{(1)}}}{2} a_1, \tag{A9}$$

as well as

$$b_R^{out(1)} = b^{out} - \frac{\sqrt{\gamma_L^{(2)}}}{2} a_2 \tag{A10}$$

and

$$b_L^{out(2)} = b^{out} - \frac{\sqrt{\gamma_R^{(1)}}}{2} a_1. \tag{A11}$$

We may now rewrite Eqs. (A1)–(A4) in the fields and note that

$$b_R^{in(1)} + b_R^{out(1)} = b_L^{in(2)} + b_L^{out(2)} = b^{in} + b^{out}, \tag{A12}$$

as well as

$$b_R^{out(1)} - b_R^{in(1)} = \sqrt{\gamma_R^{(1)}} a_1 \tag{A13}$$

and

$$b_L^{out(2)} - b_L^{in(2)} = \sqrt{\gamma_L^{(2)}} a_2. \tag{A14}$$

Equations (A5), (A6), (A13), and (A14) express photon number conservation at the respective mirror: an incident photon can either be transferred into the cavity or be reflected. This interpretation is easily verified (omitting unnecessary indices) by considering the change of cavity photon number $a^\dagger a$ by a single mirror (interface). For a nonabsorbing linear interface and using retarded and/or advanced solutions one obtains, using Eqs. (A1)–(A4),

$$\frac{d}{dt}(a^\dagger a)|_{inter\ face} = -\sqrt{\gamma} b^{out\dagger} a + \sqrt{\gamma} a^\dagger b^{in}, \tag{A15}$$

$$\frac{d}{dt}(a^\dagger a)|_{inter\ face} = \sqrt{\gamma} b^{in\dagger} a - \sqrt{\gamma} a^\dagger b^{out},$$

$$\frac{d}{dt}(a^\dagger a)|_{inter\ face} = -\gamma a^\dagger a + \sqrt{\gamma}(a^\dagger b^{in} + b^{in\dagger} a), \tag{A16}$$

or, equivalently,

$$\frac{d}{dt}(a^\dagger a)|_{inter\ face} = \gamma\gamma a^\dagger a - \sqrt{\gamma}(a^\dagger b^{out} + b^{out\dagger} a).$$

They express the conversion between cavity mode $a$ and *in* and *out* channel states. The requirement of equivalence of these four expressions leads to relations of the form (A13) and (A14) once proper *in* and *out* channel states have been identified. In particular, Eqs. (A8)–(A11) define the proper channel states for the central photon bath.

Photon number conservation in the central bath region imposes the conditions $b_R^{in(1)}(\omega) = b_L^{out(2)}(\omega)\exp\{i\omega t_{prop}\}$ and $b_L^{in(2)}(\omega) = b_R^{out(1)}(\omega)\exp\{i\omega t_{prop}\}$. In this paper, we use

$$b_R^{in(1)}(\omega) = \kappa(\omega) b_L^{out(2)}(\omega) \tag{A17}$$

and

$$b_L^{in(2)}(\omega) = \kappa(\omega) b_R^{out(1)}(\omega) \tag{A18}$$

with the simple filter function $\kappa(\omega) = \kappa_0 \exp i\omega t_{prop}$, $0 \leqslant \kappa_0 \leqslant 1$, to account for the time delay $t_{prop}$ and absorptive losses in the central bath between the two cavities. A clean treatment of dissipative losses between the cavities may be achieved by treating this region as a quantized dispersive medium.[29]

The Fourier transformed kinetic equations for the driven cavity fields are

$$a_1(\omega)\mathcal{N}_1(\omega) = -\sqrt{\gamma_L^{(1)}} b_L^{in(1)}(\omega) - \sqrt{\gamma_R^{(1)}} b_R^{in(1)}(\omega) \tag{A19}$$

and

$$a_2(\omega)\mathcal{N}_2(\omega) = -\sqrt{\gamma_L^{(2)}} b_L^{in(2)}(\omega) - \sqrt{\gamma_R^{(2)}} b_R^{in(2)}(\omega), \tag{A20}$$

using the definitions of $\mathcal{N}_i(\omega)$ as used in Eq. (7).

Elimination of the cavity modes, as well as the modes $b$ in the central bath region gives $b_R^{out(2)}(\omega)$ in terms of $b_R^{in(2)}(\omega)$ and $b_L^{in(1)}(\omega)$, as well as $b_L^{out(1)}(\omega)$ in terms of $b_L^{in(1)}(\omega)$ and $b_R^{in(2)}(\omega)$, leading to the $S$ matrix given in Eq. (9) and, equivalently, Eq. (8).


[1] Y. Yamamoto and A. Imamoglu, *Mesoscopic Quantum Optics* (Wiley, New York, 1999).
[2] S. Haroche and J.-M. Raimond, *Exploring the Quantum-Atoms, Cavities, and Photons* (Oxford University Press, New York, 2006).
[3] A. Wojs and P. Hawrylak, Phys. Rev. B **51**, 10880 (1995).
[4] L. Jacak, P. Hawrylak, and A. Wojs, *Quantum Dots* (Springer, Berlin, 1998).
[5] K. V. Kavokin, Phys. Status Solidi A **195**, 592 (2003).
[6] I. A. Akimov, A. Hundt, T. Flissikowski, and F. Henneberger, Appl. Phys. Lett. **81**, 4730 (2002).
[7] M. Bayer, G. Ortner, O. Stern, A. Kuther, A. A. Gorbunov, A. Forchel, P. Hawrylak, S. Fafard, K. Hinzer, T. L. Reinecke, S. N. Walck, J. P. Reithmaier, F. Klopf, and F. Schäfer, Phys. Rev. B **65**, 195315 (2002).
[8] J. G. Tischler, A. S. Bracker, D. Gammon, and D. Park, Phys. Rev. B **66**, 081310(R) (2002).
[9] I. A. Akimov, K. V. Kavokin, A. Hundt, and F. Henneberger, Phys. Rev. B **71**, 075326 (2005).
[10] R. Seguin, S. Rodt, A. Schliwa, K. Pötschke, U. W. Pohl, and D. Bimberg, Phys. Status Solidi B **243**, 3937 (2006).
[11] N. I. Cade, H. Gotoh, H. Kamada, H. Nakano, and H. Okamoto,

Phys. Rev. B **73**, 115322 (2006).
[12] J. Cheng, Y. Wu, X. Xu, D. Sun, D. G. Scheel, A. S. Bracker, D. Gammon, W. Yao, and L. J. Sham, Solid State Commun. **140**, 381 (2006).
[13] M. V. Gurudev Dutt, J. Cheng, B. Li, X. Xu, X. Li, P. R. Berman, D. G. Steel, A. S. Bracker, D. Gammon, S. E. Economou, R.-B. Liu, and L. J. Sham, Phys. Rev. Lett. **94**, 227403 (2005).
[14] T. Calarco, A. Datta, P. Fedichev, E. Pazy, and P. Zoller, Phys. Rev. A **68**, 012310 (2003).
[15] S. Haroche and J.-M. Raimond, *Exploring the Quantum, Atoms, Cavities, and Photons* (University Press, Oxford, 2006), p. 231.
[16] H. Cao, *Coherent Control in Atoms, Molecules, and Semiconductors*, edited by W. Pötz and W. A. Schroeder (Kluwer, Dordrecht, 1999), pp. 157–168.
[17] H. J. Krenner, S. Stufler, M. Sabathil, E. C. Clark, P. Ester, M. Bichler, G. Abstreiter, J. J. Finley, and A. Zrenner, New J. Phys. **7**, 184 (2005).
[18] D. Loss and D. P. DiVincenzo, Phys. Rev. A **57**, 120 (1998).
[19] W. D. Oliver, F. Yamaguchi, and Y. Yamamoto, Phys. Rev. Lett. **88**, 037901 (2002).
[20] C. Simon, Y.-M. Niquet, X. Caillet, J. Eymery, J.-P. Poizat, and J.-M. Gerard, Phys. Rev. B **75**, 081302(R) (2007).
[21] T. D. Ladd, P. van Loock, K. Nemoto, W. J. Munro, and Y. Yamamoto, New J. Phys. **8**, 184 (2006).
[22] M. Atatüre, J. Dreiser, A. Badolato, and A. Imamoglu, Nat. Phys. **3**, 101 (2007).
[23] K. Hennessy, A. Badolato, M. Winger, D. Gerace, M. Atatüre, S. Gulde, S. Fält, E. L. Hu, and A. Imamoglu, Science **312**, 551 (2006).
[24] W. Schäfer and M. Wegener, *Semiconductor Optics and Transport Phenomena* (Springer, Berlin, 2002).
[25] C. W. Gardiner and M. J. Collett, Phys. Rev. A **31**, 3761 (1985).
[26] D. F. Walls and G. J. Milburn, *Quantum Optics* (Springer, Berlin, 1995), p. 121.
[27] G. Lindblad, Commun. Math. Phys. **48**, 119 (1976).
[28] See, for example, W. Pötz, J. Math. Phys. **36**, 1707 (1995).
[29] S. Scheel, L. Knöll, and D.-G. Welsch, Phys. Rev. A **60**, 4094 (1999).
[30] P. Meystre and M. Sargent III, *Elements of Quantum Optics*, 3rd ed. (Springer, Berlin, 1999).
[31] G. Bester, S. Nair, and A. Zunger, Phys. Rev. B **67**, 161306(R) (2003).
[32] E. O. Kane, in *Semiconductors and Semimetals, Physics of III-V Compounds*, edited by R. K. Willardson and A. C. Beer (Academic, New York, 1966), Vol. 1, p. 75.
[33] R. G. Newton, *Scattering Theory of Waves and Particles* (McGraw-Hill, New York, 1966).
[34] J. Grond, W. Pötz, and A. Imamoglu (unpublished).
[35] W. Pötz, Proceedings of IWCE-12, Amherst, October 2007 (unpublished).